

K-Shell Photoionization of Singly Ionized Atomic Nitrogen: Experiment and Theory

M F Gharaibeh¹†, J M Bizau^{2,3}, D Cubaynes^{2,3}, S Guilbaud², N El Hassan², M M Al Shorman², C Miron³, C Nicolas³, E Robert³, C Blancard⁴ and B M McLaughlin^{5,6}‡

¹Department of Physics, Jordan University of Science and Technology, Irbid 22110, Jordan.

²Institut des Sciences Moléculaires d'Orsay (ISMO), CNRS UMR 8214, Université Paris-Sud, Bât. 350, F-91405 Orsay cedex, France

³Synchrotron SOLEIL - L'Orme des Merisiers, Saint-Aubin - BP 48 91192 Gif-sur-Yvette cedex, France

⁴CEA-DAM-DIF, Bruyères-le-Châtel, F-91297 Arpajon Cedex, France

⁵Centre for Theoretical Atomic, Molecular and Optical Physics (CTAMOP), School of Mathematics and Physics, Queen's University Belfast, Belfast BT7 1NN, Northern Ireland, UK

⁶Institute for Theoretical Atomic and Molecular Physics (ITAMP), Harvard Smithsonian Center for Astrophysics, MS-14, Cambridge, MA 02138, USA

Abstract. Absolute cross sections for the K-shell photoionization of C-like nitrogen ions were measured by employing the ion-photon merged-beam technique at the SOLEIL synchrotron radiation facility in Saint-Aubin, France. High-resolution spectroscopy with $E/\Delta E \approx 7,000$ was achieved with the photon energy from 388 to 430 eV scanned with a band pass of 300 meV, and the 399.4 to 402 eV range with 60 meV. Experimental results are compared with theoretical predictions made from the multi-configuration Dirac-Fock (MCDHF) and R-matrix methods. The interplay between experiment and theory enabled the identification and characterization of the strong $1s \rightarrow 2p$ resonances observed in the spectra.

PACS numbers: 32.80.Fb, 31.15.Ar, 32.80.Hd, and 32.70.-n

Short title: K-shell photoionization of N^+ ions

Draft for J. Phys. B: At. Mol. & Opt. Phys: 2 April 2021

† Corresponding author, E-mail: mfg@just.edu.jo

‡ Corresponding author, E-mail: b.mclaughlin@qub.ac.uk

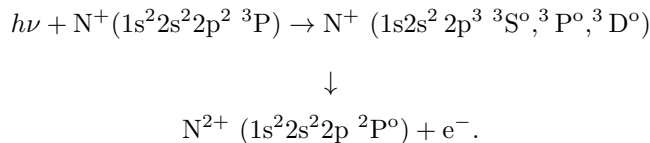
1. Introduction

Satellites *Chandra* and *XMM-Newton* currently provide a wealth of X-ray spectra of astronomical objects; however, a serious lack of high-quality atomic data impedes the interpretation of these spectra [1, 2, 3, 4, 5]. Recent studies on Carbon and its ions have shown that high quality data is required to model the observations in the X-ray spectrum of the bright blazar Mkn 421 observed by the Chandra LETG+HRC-S [6]. Spectroscopy in the soft X-ray region (5-45 Å) including K-shell transitions of C, N, O, Ne, S and Si, in neutral, singly or doubly ionized states and L-shell transitions of Fe and Ni, provides a valuable tool for probing the extreme environments in active galactic nuclei (AGN's), X-ray binary systems, cataclysmic variable stars (CV's) and Wolf-Rayet Stars [7] as well as the interstellar media (ISM) [8]. The latter, recent work, for example, demonstrated that X-ray spectra from *XMM-Newton* can be used to characterize ISM, provided accurate atomic oxygen *K*-edge cross sections are available. Analogous results concerning the chemical composition of the ISM are to be expected with the availability of accurate data on neutral [9, 10] and singly ionized atomic nitrogen *K*-edge cross sections. The globular cluster X-ray source CXO J033831.8-352604 in NGC 1399 has also recently been found to show strong emission lines of [O III] and [N II] in its optical spectrum in addition to ultraluminous X-ray emission with a soft X-ray spectrum [11, 12].

This lack of available X-ray data has motivated not only the present authors to perform K-shell photoionization studies on such ions but also other groups who use the same or similar experimental techniques. K-shell photoionization cross section results have been obtained on a variety of ions of astrophysical interest; He-like Li⁺ [13, 14], Li-like B²⁺ [15], C³⁺ [16], Be-like B⁺ [17], C²⁺ [18], B-like C⁺ [19], N-like O⁺ [20], F-like Ne⁺ [21], along with valence shell studies on Mg-like Fe¹⁴⁺ [22]. The majority of this experimental data has been benchmarked with state-of-the-art theoretical methods.

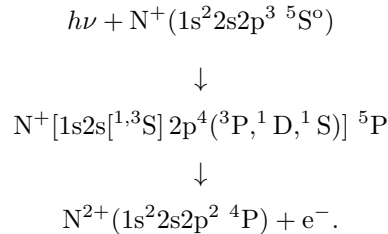
The present work on this proto-type C-like ion provides benchmark values for cross sections on photoabsorption of X-rays in the vicinity of the *K*-edge, where strong n=2 inner-shell resonance states of singly ionized atomic nitrogen are observed. No experiments have been reported to date on singly ionized atomic nitrogen in the *K*-edge photon energy region, previous experimental studies have been restricted to the valence shell region [23].

Promotion of a K-shell electron in C-like nitrogen (N⁺) ions to an outer np-valence shell (1s → np) from the ground state produces states that can autoionize, forming a N²⁺ ion and an outgoing free electron. One of the strongest excitation processes in the interaction of a photon with the 1s²2s²2p² ³P ground-state of the C-like nitrogen ion is the 1s → 2p photo-excitation process;



Experimental studies of this singly ionized atomic nitrogen ion in its ground state 1s²2s²2p² ³P are further hampered by the presence of metastable states as the N⁺ ions are produced in the gas-phase using an Electron-Cyclotron-Resonance-Ion-Source (ECRIS). Metastable states 1s²2s²2p² ¹D, ¹S, and 1s²2s2p³ ⁵S^o are present in the ion

beam. In the case of the $1s^2 2s 2p^3 \ ^5S^\circ$ metastable state auto-ionization processes occurring by the $1s \rightarrow 2p$ photo-excitation process are;



Similarly, auto-ionization processes may also occur for the $1s^2 2s^2 2p^2 \ ^1D, \ ^1S$ metastable states interacting with photons. To our knowledge this would appear to be the first time experimental measurements have been performed on this proto-type C-like system in the photon energy region of the *K*-edge.

Theoretical photoionization (PI) cross section calculations for inner-shell processes in this C-like ion have been performed by Reilman and Manson [24] using the Hartree-Slater wavefunctions of Herman and Skillman [25] and by Verner and co-workers [26] using Dirac-Slater potentials ([27, 28]) within a central field approximation. Photoionization cross sections obtained using these methods may be suitably accurate at very high photon energies but often give poor results near thresholds where configuration mixing is strong and resonance structure prevails, as is the case for the processes investigated here in the vicinity of the *K*-edge threshold. Central field methods neglect resonance features (observed in experimental measurements) as degenerate subshells of equivalent electrons rather than individual energy levels are considered. Therefore, any results obtained from these approaches in spectral modelling should be treated with due caution.

In this paper we present detailed measurements of the single and double PI cross sections in the 398 - 406 eV region (the only one where peaks were observed) from the entire 388 - 430 eV photon energy range explored. Our MCDF and R-matrix calculations enabled the identification and characterization of the strong $1s \rightarrow 2p$ resonances observed in the spectra. The present investigation provides absolute values (experimental and theoretical) for PI cross sections, $n=2$ inner-shell resonance energies and linewidths occurring in the interaction of a photon with the $1s^2 2s^2 2p^2 \ ^3P, \ ^1D, \ ^1S$, and $1s^2 2s 2p^3 \ ^5S^\circ$ states of the N^+ ion.

The layout of this paper is as follows. Section 2 details the experimental procedure used. Section 3 presents a brief outline of the theoretical work. Section 4 presents a discussion of the results obtained from both the experimental and theoretical methods. Finally in section 5 conclusions are drawn from the present investigation.

2. Experiment

2.1. Ion production

The present measurements were made using the new MAIA (Multi-Analysis Ion Apparatus) set-up, figure 1, permanently installed on Branch A of the PLEIADES beam line [29] at SOLEIL, the French national synchrotron radiation facility, located in Saint-Aubin, France. It is a merged beam set-up, similar to the one originally designed by Peart *et al* [30] for measuring electron impact cross sections. A simplified scheme of the set-up is shown in figure 1.

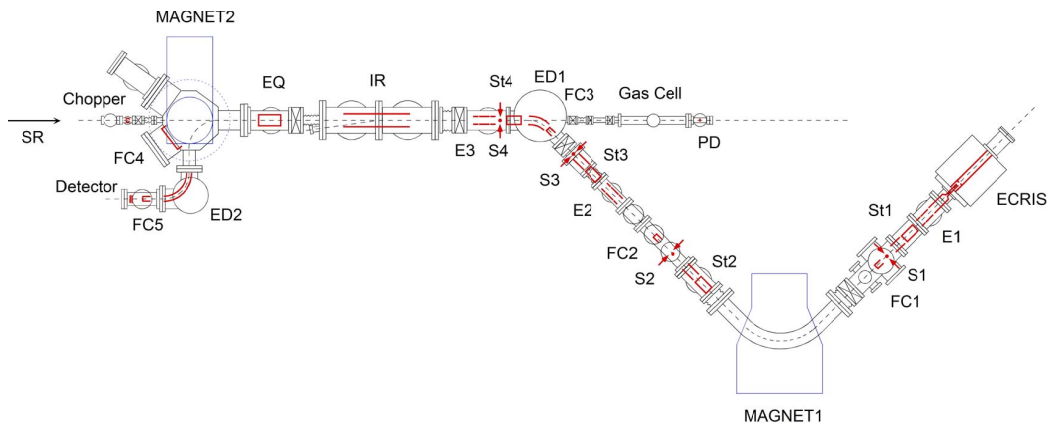


Figure 1. (Colour online) Scheme of the MAIA set-up on the PLEIADES beam line. The ionic optics used for the ion beam transport are represented in red. ECRIS: Electron Cyclotron Ion Source, E: einzel lens, St: set of horizontal and vertical steerers, S: collimating slits, FC: Faraday cup, ED: electrostatic deflector, IR: interaction region, EQ: electrostatic quadrupole, SR: synchrotron radiation, PD: photodiode.

The N^+ ions are produced in a permanent magnet Electron Cyclotron Resonance Ion Source (ECRIS) especially designed for this set-up at the CEA (Commissariat à l’Energie Atomique et aux Energies Alternatives) in Grenoble and previously tested at LURE (Laboratoire pour l’Utilisation de Rayonnement Electromagnétique) in Orsay [31]. To produce a nitrogen plasma, molecular nitrogen gas is injected into the plasma chamber and heated by a 12.6 GHz micro-wave. A power of a few watts is sufficient for an optimum production of the N^+ ions. The ions are extracted by applying a 2 kV bias on the source and selected in mass/charge ratio by a dipole magnet. The selected ions are deflected by a 45° spherical electrostatic deflector (ED1) to be merged with the photon beam inside a 50 cm long interaction region (IR). Two sets of slits (S2 and S3) allow the matching of the size of the ion beam to the size of the photon beam. After interaction, the charge of the ions is analyzed by a second dipole magnet. The parent ions are collected in a Faraday cup (FC4), and the so-called photoions which have gained one (or several) charge(s) are counted using channel-plates.

2.2. Excitation source

The photon beam is monochromatized synchrotron radiation from the PLEIADES beam line. Two undulators with 256 mm and 80 mm period deliver photons in the 10 - 100 eV and 100 eV - 1000 eV energy ranges, respectively, with all types of polarization above 55 eV. The light is monochromatized by a plane grating monochromator with no entrance slit. High spectral purity is obtained by a combination of a quasi-periodic design for the undulators and the use of a varied groove depth for the plane grating. Three varied line spacing gratings are available for the adjustment of the resolution. An ultimate resolving power of approximately 10^5 is achievable at 50 eV. After monochromatization, the light is distributed and focalized to three different branches. On branch A, used for this experiment, the photon beam is parallel, with a typical spot size of 2 mm \times 2 mm. The photon flux is measured using a calibrated silicon photodiode (PD). The photon energy is determined using a double-ionization chamber of the Samson type [32]. For this work, we used the $1s \rightarrow \pi^*$ transitions in the N_2 gas [33] and $2p \rightarrow 3d$ transitions in Ar gas [34] for calibration purposes. The photon energy was corrected for Doppler shift resulting from the velocity of the N^+ ions. The estimated accuracy of the photon energy determination is 40 meV.

2.3. Experimental procedure

The merged-beam set-up allows a determination of the absolute photoionization cross sections. At a given photon energy, the cross sections σ_{PI} are obtained from:

$$\sigma_{PI} = \frac{Se^2\eta\nu q}{IJ\epsilon \int_0^L \frac{dz}{\Delta x \Delta y F(z)}} \quad (1)$$

where S is the counting rate of photoions measured with the channel-plates and η is the efficiency of the photodiode. A chopper, placed at the exit of the photon beam line, allows to subtract from the photoions signal, the noise produced by collisional ionization processes, charge stripping on the slits or autoionizing decay of metastable excited states of N^+ ions produced in the ECRIS. Here q is the charge of the target ions; ν is the velocity of the ions in the interaction region determined from the accelerating potential applied to the ECRIS; I is the current produced by the photons on the calibrated photodiode. The efficiency η of the photodiode was calibrated in the 10-1000 eV energy range at the Physikalisch-Technische Bundesanstalt (PTB) beam line at BESSY in Berlin; e is the charge of the electron; J is the current of incident ions measured in FC4; ϵ is the efficiency of the microchannel plates determined by comparing the counting rate produced by a low intensity ion beam and the current induced by the same beam in FC4; $\Delta x \Delta y F(z)$ is an effective beam area (z is the propagation axis of the two beams), and $F(z)$ is a two dimensional form factor determined using three sets of xy scanners placed at each end and in the middle of the interaction region. Each scanner is a 0.2 mm width slit moved across the ion and the photon beams. The length L of the interaction region is fixed by applying a 200 V bias on a 50 cm long tube placed in the interaction region, resulting in a different velocity for the photoions produced inside and outside the tube. $F(z)$ is defined by:

$$F_{xy} \approx \frac{\sum i_{xy} \sum j_{xy}}{\sum \sum i_{xy} j_{xy}} \quad (2)$$

where $i_{xy} = i(x,y)\Delta x \Delta y$ and $j_{xy} = j(x,y)\Delta x \Delta y$ are the ion and photon currents, respectively, passing through the slits and measured with FC4 for the ion beam and

Table 1. Typical values for the experimental parameters involved in evaluating the absolute cross section measured at a photon energy of 400 eV.

S	30 Hz
Noise	17 Hz
ν	$1.6 \cdot 10^5$ m/s
Photon flux	$4.1 \cdot 10^{11}$ s ⁻¹
J	38 nA
ϵ	0.62
F_{xy}	30

the photodiode for the photon beam, and Δx and Δy are the step sizes used to scan the slits, typically 0.2 mm. Typical values of the parameters involved in equation (1), measured at a photon energy of 400 eV are given in table 1. The contribution of N_2^{2+} molecular ions in the incident beam was subtracted. It was measured after the beam time using ^{14}N ^{15}N isotopic gas to be of the order of 3 %.

The accuracy of the measured cross-sections is determined by statistical fluctuations on the photoion and noise counting rates and a systematic contribution resulting from the measurement of the different parameters in equation (1). The latter is estimated to be 15% and is dominated by the uncertainty on the determination of the photon flux, the form factor and detector efficiency.

To record the single (double) photoionization spectra, the field in the dipole magnet was adjusted to detect N^{2+} ions (N^{3+} ions) with the channel-plates as the photon energy was scanned. Two modes have been used. One with no voltage applied on the interaction tube, allowing a better statistic since the whole interaction length of the beams is used. In this mode only relative cross sections are obtained. In the second mode, the voltage is applied to the tube to define the interaction length L (50 cm), which allows the determination of the cross sections in absolute value.

3. Theory

3.1. MCDF

We have performed multi-configurational Dirac-Fock (MCDF) calculations based on full intermediate coupling in a jj basis using the code developed by Bruneau [35]. The photoexcitation cross sections involving $1s \rightarrow np$ transitions have been considered for all the levels of the N^+ ground configuration, namely $1s^2 2s^2 2p^2$ $^3P_{0,1,2}$, 1D_2 and 1S_0 . The metastable $1s^2 2s 2p^3$ $^5S_2^o$ level also has been considered. The calculations were limited to principal quantum number up to 4.

Only electric dipole transitions have been computed using Babushkin and Coulomb gauges, respectively. The oscillator strengths obtained in the two gauges differ by less than 10%. Using the MCDF code we have calculated the average autoionization rate Γ_{av} (meV) of the $1s 2s^2 2p^3$ configuration (with a $1s$ vacancy) to be equal to 96 meV (which corresponds to a lifetime τ of 3.43 femto-seconds (fs) from the uncertainty principle $\Delta E \Delta t = \hbar/2$). From the MCDF calculations synthetic spectra are constructed as a sum of lorentzian profiles using, for all the lines, the Γ_{av} value as the full width at half maximum (FWHM). In order to compare directly with the experimental measurements made at 300 meV and 60 meV the MCDF results were convoluted with gaussian functions of FWHM of 300 meV and

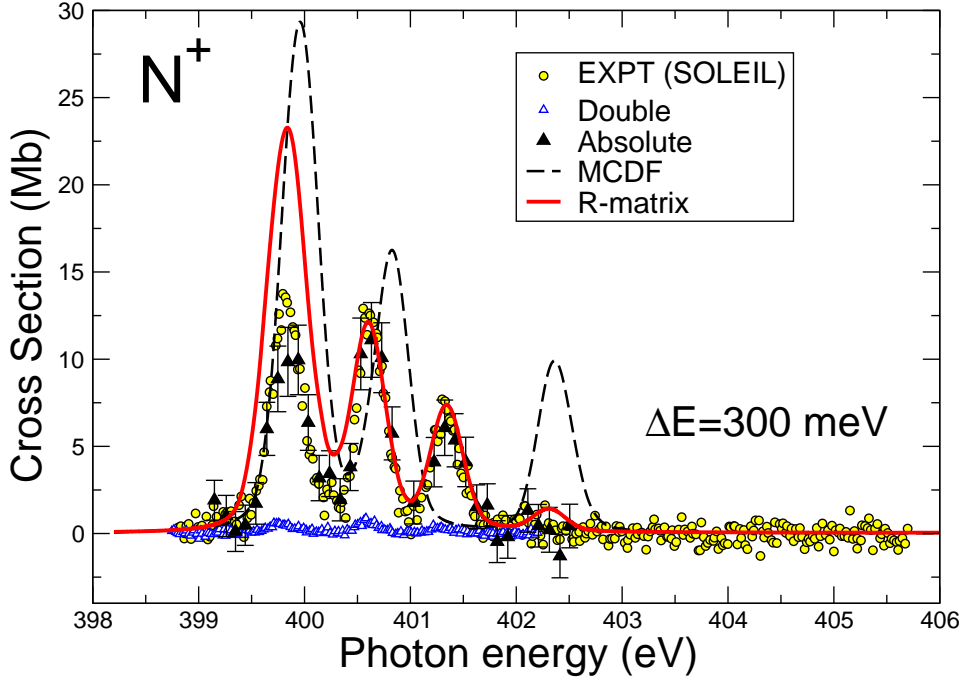


Figure 2. (Colour online) Photoionization cross sections measured with a 300 meV band pass. Open circles : single photoionization. The absolute measurements (solid black triangles), single photoionization have been obtained with a larger energy step. Open blue triangles: double photoionization. The error bars give the total uncertainty of the experimental data. The MCDF (dashed line) and R-matrix (solid line) calculations shown were obtained by convolution with a Gaussian profile of 300 meV FWHM and a weighting of the states (see text for details) to simulate the measurements.

60 meV respectively, to simulate the measurements. A non-statistical distribution of the ground and metastable states gave best agreement with experiment by weighting the contribution of the $1s^2 2s^2 2p^2$ $^3P, ^1D, ^1S$, and $1s^2 2s 2p^3$ $^5S^o$ states by (0.54, 0.11, 0.03, 0.32) respectively.

3.2. R-Matrix

The R-Matrix method [36, 37, 38], with an efficient parallel implementation of the codes [39] was used to determine all the PI cross sections, for both the initial 3P ground state and the, 1S , 1D and $^5S^o$ metastable states in LS -coupling using 390-levels in the close-coupling expansion. The Hartree-Fock 1s, 2s and 2p tabulated orbitals of Clementi and Roetti [40] were used together with the $n=3$ orbitals of the N^{2+} ion determined by energy optimization on the appropriate hole-shell state

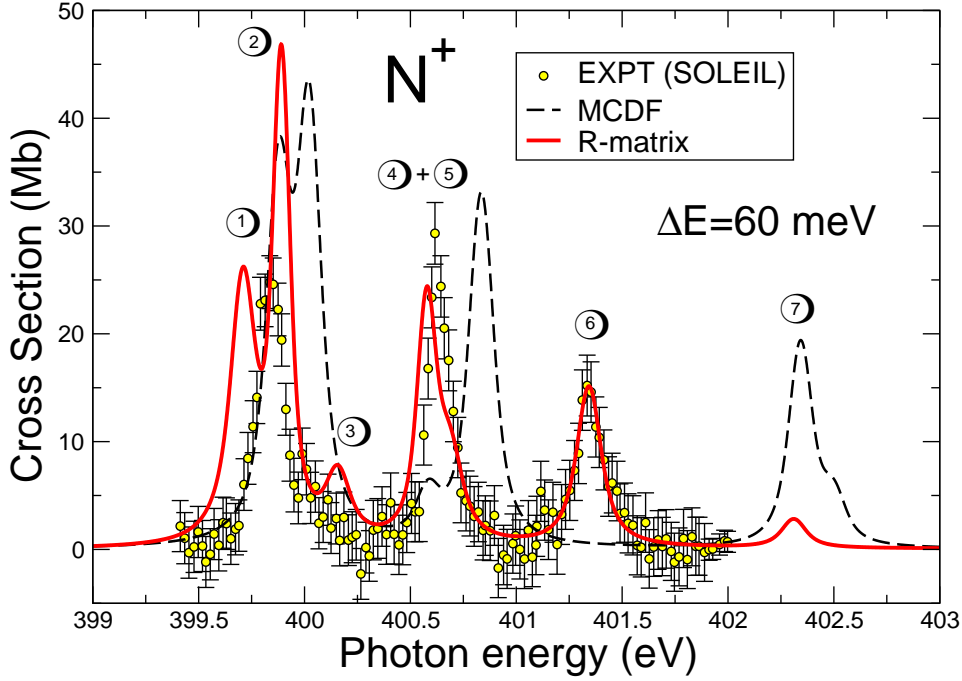


Figure 3. (Colour online) Comparison of the single photoionization cross section (yellow circles) measured with 60 meV band pass (points with error bar giving the statistical uncertainty). The MCDF (dashed line) and R-matrix (solid line), calculations shown were obtained by convolution with a Gaussian profile of 60 meV FWHM and a weighting of the states (see text for details) to simulate the measurements. Table 2 gives designation of the resonances ① - ⑦,

using the atomic structure code CIV3 [41]. The $n=3$ correlation (pseudo) orbitals are included to account for core relaxation and additional correlation effects in the multi-configuration interaction wavefunctions. All the N^{2+} residual ion states were then represented by using multi-configuration interaction wave functions. The non-relativistic R -matrix approach was used to calculate the energies of the N^+ bound states and the subsequent PI cross sections. PI cross sections out of the $1s^2 2s^2 2p^2$ 3P ground state and the 1S , 1D along with the $1s^2 2s 2p^3$ $^5S^o$ metastable states were then obtained for all total angular momentum scattering symmetries that contribute.

All our PI cross sections were determined in LS - coupling with the parallel version [39] of the R-matrix programs [36, 37, 38] and 390 levels of the N^{2+} residual ion included in our close-coupling calculations. Due to the presence of meta stable states in the beam, PI cross-section calculations were performed for both the $1s^2 2s^2 2p^2$ 3P ground state and the $1s^2 2s^2 2p^2$ 1S , 1D and $1s^2 2s 2p^3$ $^5S^o$ meta stable states of the N^+ ion. Here again, in order to compare directly with the experimental

measurements made at 300 meV and 60 meV the R-matrix results were convoluted with gaussian functions of FWHM of 300 meV and 60 meV respectively, to simulate the measurements. A non-statistical distribution of the ground and metastable states gave best agreement with experiment by weighting the contribution of the $1s^2 2s^2 2p^2 \ ^3P, \ ^1D, \ ^1S$, and $1s^2 2s 2p^3 \ ^5S^o$ states by (0.54, 0.11, 0.03, 0.32) respectively.

The scattering wavefunctions were generated by allowing all possible two-electron promotions out of select base configurations of N^+ into the orbital set employed. Scattering calculations were performed with twenty continuum functions and a boundary radius of 6.2 Bohr radii. For both the $\ ^3P$ ground state and the $\ ^1S, \ ^1D, \ ^5S^o$ metastable states the outer region electron-ion collision problem was solved (in the resonance region below and between all the thresholds) using a suitably chosen fine energy mesh of 2×10^{-7} Rydbergs ($\approx 2.72 \ \mu\text{eV}$) to fully resolve all the resonance structure in the PI cross sections. Radiation and Auger damping were also included in the cross section calculations. Finally the total spectrum was obtained assuming a weighting of the $1s^2 2s^2 2p^2 \ ^3P, \ ^1D, \ ^1S$, and $1s^2 2s 2p^3 \ ^5S^o$ states by (0.54, 0.11, 0.03, 0.32) respectively in order to compare directly with the PI cross section measurements obtained using the ion beam produced from the ECRIS at the SOLEIL radiation facility.

The multi-channel R-matrix QB technique (applicable to atomic and molecular complexes) of Berrington and co-workers [42, 43, 44] was used to determine the resonance parameters. The resonance width Γ may be determined from the inverse of the energy derivative of the eigenphase sum δ at the position of the resonance energy E_r via

$$\Gamma = 2 \left[\frac{d\delta}{dE} \right]_{E=E_r}^{-1} = 2[\delta']_{E=E_r}^{-1} . \quad (3)$$

The results for the resonance parameters determined from the QB method are presented in Table 2.

4. Results and Discussion

In the entire 388-430 eV photon energy range we explored, only three intense structures were observed around 400 eV. Figure 2 shows our experimental and theoretical (MCDF and R-matrix) results over the photon energy range 398 eV – 406 eV. The experimental results were taken with a photon energy resolution of 300 meV. The black triangles show the measurements of the single PI cross section obtained in the absolute mode. The yellow circles have been obtained in the relative mode with a smaller energy step. They have been put on the absolute scale keeping the same area under the absolute and relative measurements. The open blue triangles give the double PI cross section determined in the relative mode. To place them on the absolute scale it was assumed that the length of the interaction region was the same while recording the relative single and double PI cross sections.

In order to compare directly with the experimental measurements both our MCDF and R-matrix results were convoluted with a gaussian function of FWHM of 300 meV to simulate the measurements. Furthermore, we found that a non-statistical distribution of the ground and metastable states gave best agreement with experiment by weighting the contribution of the $1s^2 2s^2 2p^2 \ ^3P, \ ^1D, \ ^1S$, and $1s^2 2s 2p^3 \ ^5S^o$ states by (0.54, 0.11, 0.03, 0.32) respectively. A statistical weighting showed greater disparity between theory and experiment. Figure 3 shows the same experimental and theoretical

(MCDF and R-matrix) single PI cross sections results over the photon energy range 399 eV – 403 eV but at the higher resolution of 60 meV. Voigt profiles were used to fit the peaks in the experimental data, to extract the linewidths, assuming a Gaussian instrumental contribution of 60 meV for each peak. The experimental data, obtained in the relative mode, were normalised keeping the same total area under the experimental single PI cross section measured with 60 meV and 300 meV band pass (yellow circles on figures 2 and 3). The error bars give the statistical uncertainty. The measured double PI cross section is only 4% of the single PI, these data are shown in figure 2 by the open blue triangles. Here again theory has been convoluted with a gaussian of 60 meV FWHM and the weighting of the states used as before. Both MCDF and R-matrix calculations are in good qualitative agreement with the experimental results. The position of the lines is better described by the R-matrix calculations, from matching the calculated and experimental ionization thresholds. The R-matrix calculations include Auger and radiation damping, missing from the MCDF calculations and give lines intensity in closer agreement with experiment. The R-matrix calculations indicate radiation damping can contribute up to 30%.

In Table 2 we present the MCDF theoretical values for the resonance energies and linewidths from our work which were obtained by fitting the various peaks found in the cross sections to Fano profiles for overlapping resonances. This enabled the extraction of the resonance energies and natural linewidths for the various states. The assignment of the peaks in the PI cross sections (due to $1s \rightarrow 2p$ photo-excitation) is based on our R-matrix theoretical work, since it was not possible to extract experimental values for each individual state as the lines are a blend of different states. The first strong peak at about 399.85 eV is primarily a blend of the resonance ①, $1s2s^22p^3\ ^3D^o$, resulting from photo-excitation of the ground $1s^22s^22p^2\ ^3P$ state along with that from resonance ②, $1s2s2p^4\ ^5P$ from the $1s^22s2p^3\ ^5S^o$ metastable state. This is clearly seen in the higher resolution experimental data taken at 60 meV (figure 3) as opposed to the measurements made at the lower resolution of 300 meV (figure 2). The valley between the first and second peak is filled with the $1s2s^22p^3\ ^1P^o$ resonance ③ resulting from photo-excitation of the $1s^22s^22p^2\ ^1S$ metastable. The next strong peak at about 400.63 eV is a blend of the $1s2s^22p^3\ ^3S^o$ resonance ④, resulting from photo-excitation from the ground $1s^22s^22p^2\ ^3P$ and the $1s2s^22p^3\ ^1D^o$ resonance ⑤, caused by photo-excitation of the $1s^22s^22p^2\ ^1D$ metastable state. The third peak at about 401.35 eV is due to the resonance ⑥, $1s2s^22p^3\ ^3P^o$, resulting from photo-excitation of the $1s^22s^22p^2\ ^3P$ ground state. Finally a broad resonance peak ⑦, at about 402.3 eV (barely visible in the experimental data, figure 2), resulting from the photo-excitation of the $1s^22s^22p^2\ ^1D$ metastable is assigned to the $1s2s^22p^3\ ^1P^o$ resonance state. These assignments are summarized in the first column of Table 2.

Experimental linewidths were extracted from the ion-yield measurements in figure 3 by fitting Voigt profiles to the peaks assuming a Gaussian instrumental contribution of 60 meV for each peak. The first resonance peak in the experimental data at 399.844 ± 0.04 eV has a linewidth of 138 ± 41 meV, the second peak located at 400.633 ± 0.04 eV has a linewidth 86 ± 10 meV and the third peak at 401.346 ± 0.04 has a linewidth of 143 ± 21 meV. The linewidth gives only an upper limit of the natural width since several lines can contribute to the structures. According to the R-matrix calculations, only peak 3 in the experimental data is pure, and following MCDF calculations, only peak 2, which may be due to the $S \rightarrow P$ dipole selection rules. Table 2 presents the theoretical results for the resonance positions and widths from our present investigations. For comparison purposes we have also included the results

Table 2. Resonance energies $E_{\text{ph}}^{(\text{res})}$ (eV), and the natural linewidths Γ (meV) for the core photoexcited $n=2$ states of N^+ ions in the photon energy region 399 eV to 403 eV. The experimental uncertainty is ± 40 meV for the resonance energies. The earlier MCDF calculations of Chen and co-workers [45] are included for comparison purposes.

Resonance (Label)		SOLEIL (Experiment [†])	R-matrix (Theory)	MCDF (Theory)
$1s^2 2s^2 2p^2 \ ^3P \rightarrow 1s 2s^2 2p^3 \ ^3D^o$ ①	$E_{\text{ph}}^{(\text{res})}$	–	399.706 ^a	399.894 ^b 394.665 ^c
	Γ	–	124 ^a	78 ^b 207 ^c
$1s^2 2s 2p^3 \ ^5S^o \rightarrow 1s 2s 2p^4 \ ^5P$ ②	$E_{\text{ph}}^{(\text{res})}$	–	399.891 ^a	400.834 ^b 401.568 ^c
	Γ	–	62 ^a	104 ^b 43 ^c
Average ① + ②	$E_{\text{ph}}^{(\text{res})}$	$399.844 \pm 0.04^\dagger$	399.799 ^d	400.364 ^e
	Γ	$138 \pm 41^\dagger$	93 ^d	91 ^e
$1s^2 2s^2 2p^2 \ ^1S \rightarrow 1s 2s^2 2p^3 \ ^1P^o$ ③	$E_{\text{ph}}^{(\text{res})}$	–	400.159 ^a	400.583 ^b 400.146 ^c
	Γ	–	115 ^a	106 ^b 164 ^c
$1s^2 2s^2 2p^2 \ ^3P \rightarrow 1s 2s^2 2p^3 \ ^3S^o$ ④	$E_{\text{ph}}^{(\text{res})}$	–	400.579 ^a	399.999 ^b 396.13 ^c
	Γ	–	78 ^a	64 ^b 122 ^c
$1s^2 2s^2 2p^2 \ ^1D \rightarrow 1s 2s^2 2p^3 \ ^1D^o$ ⑤	$E_{\text{ph}}^{(\text{res})}$	–	400.681 ^a	400.031 ^b 397.859 ^c
	Γ	–	105 ^a	108 ^b 170 ^c
Average ④ + ⑤	$E_{\text{ph}}^{(\text{res})}$	$400.633 \pm 0.04^\dagger$	400.630 ^d	400.015 ^e
	Γ	$86 \pm 10^\dagger$	92 ^d	86 ^e
$1s^2 2s^2 2p^2 \ ^3P \rightarrow 1s 2s^2 2p^3 \ ^3P^o$ ⑥	$E_{\text{ph}}^{(\text{res})}$	$401.346 \pm 0.04^\dagger$	401.347 ^a	402.342 ^b 396.430 ^c
	Γ	$143 \pm 21^\dagger$	121 ^a	110 ^b 200 ^c
$1s^2 2s^2 2p^2 \ ^1D \rightarrow 1s 2s^2 2p^3 \ ^1P^o$ ⑦	$E_{\text{ph}}^{(\text{res})}$	–	402.320 ^a	402.503 ^b 399.619 ^c
	Γ	–	132 ^a	107 ^b 164 ^c

[†]SOLEIL, experimental lines are not pure, see text for discussion.

^aR-matrix LS -coupling, present work.

^bMCDF, present work.

^cMCDF, Chen and co-workers. [45]

^dAverage R-matrix, present work

^eAverage MCDF, present work

from the earlier MCDF calculations of Chen and co-workers [45]. From the R-matrix results we see that the average autoionization rate for the $1s2s^22p^3$ configuration (with a $1s$ vacancy) is 112 meV compared to a value of 96 meV determined from our present MCDF calculations.

In Table 2 the results from our present theoretical predictions from both the MCDF and R-matrix methods overall indicate they are in suitable agreement with each other. Furthermore, It is seen that the R-matrix results give closer agreement with experiment for the resonance energies of all the peaks, deviating at most by 45 meV (c.f. the average for ① + ②), which is just outside the experimental error of 40 meV. All the other resonance energies from the R-matrix work are within the 40 meV experimental uncertainty however greater disparity is seen between experiment and the MCDF results. The use of a much larger basis in the R-matrix work along with coupling to the continuum could possibly improve the agreement with experiment but vastly increases the computational complexity of the problem. As seen from Table 2 discrepancies occur in the position and autoionization linewidth of the resonances from our work when compared to the early MCDF calculations of Chen et al. [45]. This was also highlighted by Garcia and co-workers [9] where outstanding discrepancies were found with that MCDF work, in particular wavelengths and A-coefficients for this C-like ion, which those authors believed to be due to numerical error by Chen et al. [45].

5. Conclusions

Photoionization of C-like nitrogen ions, N^+ , has been investigated using state-of-the-art experimental and theoretical methods. High-resolution spectroscopy was performed with $E/\Delta E = 7000$ at the SOLEIL synchrotron radiation facility, in Saint-Aubin, France, covering the energy ranges 388 eV to 430 eV where several strong peaks in the cross sections were found in the energy region around 400 eV. For these observed peaks, suitable agreement is found between the present theoretical and experimental results both on the photon-energy scale and on the PI cross-section scale for this prototype C-like system. The strength of the present study is in its excellent experimental resolving power coupled with theoretical predictions using the MCDF and R-matrix method. Given that the present results have been benchmarked with high resolution experimental data and with state-of-the-art theoretical methods they would be suitable to be included in astrophysical modelling codes such as CLOUDY [46, 47] and XSTAR [48]. The theoretical R-matrix cross sections for the individual states are available by contacting one of the authors, B M McLaughlin, b.mclaughlin@qub.ac.uk.

Acknowledgments

Data collection was performed on the PLEIADES beamline, at the SOLEIL Synchrotron radiation facility in Saint-Aubin, France. The authors would like to thank the staff of SOLEIL and, in particular, the staff of the PLEIADES beam line for their helpful assistance. The experimental research work described here has been supported by Triangle de le Physique contract 2007-001T. B M McLaughlin acknowledges support by the US National Science Foundation through a grant to ITAMP at the Harvard-Smithsonian Center for Astrophysics. The computational work was carried out at the National Energy Research Scientific Computing Center in

Oakland, CA, USA and on the Tera-grid at the National Institute for Computational Sciences (NICS) in Knoxville, TN, USA, which is supported in part by the US National Science Foundation.

- [1] McLaughlin B M 2001 *Spectroscopic Challenges of Photoionized Plasma (ASP Conf. Series vol 247)* ed Ferland, G and Savin D W (San Francisco, CA: Astronomical Society of the Pacific) p 87
- [2] Foster A, Smith R, Brickhouse N, Kallman T, Witthoef M 2010 *Space Sci. Rev.* **157** 135
- [3] Kallman T R 2010 *Space Sci. Rev.* **157** 177
- [4] Garcia J, Kallman T R and Mushotzky R F 2011 *Astrophys. J.* **731** 131
- [5] Quinet P, Palmeri P, Mendoza C, Bautista M, Garcia J, Witthoef M, Kallman T R 2011 *J. Elect. Spec. and Relat. Phenom.* **184** 170
- [6] Hasoglu M F, Abdel-Naby Sh A, and Gorczyca T W, Drake J J and McLaughlin B M 2010 *Astrophys. J.* **724** 1296
- [7] Skinner S L, Zhekov S A, Güdel M, Schmutz W, Sokal K R 2010 *Astronom. J.* **139** 825
- [8] Garcia J, Ramírez, J M, Kallman T R, Witthoef M, Bautista M A, Mendoza C, Palmeri P and Quinet P 2011 *Astrophys. J.* **731** L15
- [9] Garcia J, Kallman T R, Witthoef M, Behar E, Mendoza C, Palmeri P, Quintet P, Bautista M and Klapisch M 2009 *Astrophys. J. Supp. Ser.* **185** 477
- [10] Sant'Anna M M, Schlachter A S, Öhrwall G, Stolte W C, D W Lindle D W and McLaughlin B M 2011 *Phys. Rev. Letts.* **107** 033001
- [11] Irwin J A *et al* 2010 *Astrophys. J.* **712** L1
- [12] Warner B and Maccarone T J 2011 *Mon. Not. R. Astron. Soc.* **410** 870
- [13] Scully S W J, Álvarez I, Cisneros C, Emmons E D, Gharaibeh M F, Leitner D, Lubell M S, Müller A, Phaneuf R A, Püttner R, Schlachter A S, Schippers S, Ballance C P and McLaughlin B M 2006 *J. Phys. B: At. Mol. Opt. Phys.* **39** 3957
- [14] Scully S W J, Álvarez I, Cisneros C, Emmons E D, Gharaibeh M F, Leitner D, Lubell M S, Müller A, Phaneuf R A, Püttner R, Schlachter A S, Schippers S, Ballance C P and McLaughlin B M 2007 *J. Phys. Conf. Ser.* **58** 387
- [15] Müller A, Schippers S, Phaneuf R A, Scully S W J, Aguilar A, Cisneros C, Gharaibeh M F, Schlachter A S and McLaughlin B M 2010 *J. Phys. B: At. Mol. Opt. Phys.* **43** 135602
- [16] Müller A, Schippers S, Phaneuf R A, Scully S W J, Aguilar A, Covington A M, Álvarez I, Cisneros C, Emmons E D, Gharaibeh M F, Schlachter A S, Hinojosa G and McLaughlin B M 2009 *J. Phys. B: At. Mol. Opt. Phys.* **42** 235602
- [17] Müller A, Schippers S, Phaneuf R A, Scully S W J, Aguilar A, Cisneros C, Gharaibeh M F, Schlachter A S and McLaughlin B M 2011 *J. Phys. B: At. Mol. Opt. Phys.* in preparation
- [18] Scully S W J, Aguilar A, Emmons E D, Phaneuf R A, Halka M, Leitner D, Levin J C, Lubell M S, Püttner R, Schlachter A S, Covington A M, Schippers S, Müller A and McLaughlin B M 2005 *J. Phys. B: At. Mol. Opt. Phys.* **38** 1967
- [19] Schlachter A S, Sant'Anna M M, Covington A M, Aguilar A, Gharaibeh M F, Emmons E D, Scully S W J, Phaneuf R A, Hinojosa G, Álvarez I, Cisneros C, Müller A and McLaughlin B M 2004 *J. Phys. B: At. Mol. Opt. Phys.* **37** L103
- [20] Kawatsura K *et al* 2002 *J. Phys. B: At. Mol. Opt. Phys.* **35** 4147
- [21] Yamaoka H *et al* 2001 *Phys. Rev.* **A 65** 012709
- [22] Simon M C *et al* 2010 *Phys. Rev. Letts.* **105** 183001
- [23] Kjeldsen K *et al* 2002 *Astrophys. J. Supp. Ser.* **138** 219
- [24] Reilman R F and Manson S T 1979 *Astrophys. J. Suppl. Ser.* **40** 85
- [25] Herman F and Skillman S 1963 *Atomic Structure Calculations* (Englewood Cliffs, NJ, USA: Prentice-Hall))
- [26] Verner D A *et al* 1993 *At. Data Nucl. Data Tables* **55** 233
- [27] Slater J C 1960 *Quantum Theory of Atomic Structure* (New York, USA: McGraw-Hill)
- [28] Band I M, Kharitonov Y I and Trzhaskovskaya M B 1979 *At. Data Nucl. Data Tables* **23** 443
- [29] PLEIADES, URL www.synchrotron-soleil.fr/Recherche/LignesLumiere/PLEIADES
- [30] Peart B, Stevenson J G and Dolder K 1973 *J. Phys. B: At. Mol. Phys.* **6** 146
- [31] Bizau J M, Blancard C, Cubaynes D, Folkmann K, Champeaux J P, Lemaire J L and Wuilleumier F J 2006 *Phys. Rev. A* **73** 022718
- [32] Samson J A R 1967 *Techniques of Vacuum Ultraviolet Spectroscopy* (New York, USA: J Wiley & Sons)
- [33] Sodhi R N S and Brion C E 1977 *J. Electron Spectrosc. Relat. Phenom.* **34** 363
- [34] King G C, Tronc M, Read F H, and Bradford R C 1977 *J. Phys. B: At. Mol. Phys.* **10** 2479
- [35] Bruneau J 1984 *J. Phys. B: At. Mol. Phys.* **17** 3009
- [36] Burke P G and Berrington K A 1993 *Atomic and Molecular Processes: An R-matrix Approach*

- (Bristol, UK: IOP Publishing)
- [37] Berrington K A, Eissner W and Norrington P H 1995 *Comput. Phys. Commun.* **92** 290 URL <http://amdpp.phys.strath.ac.uk/APAP>
 - [38] Robicheaux F, Gorczyca T W, Griffin D C, Pindzola M S and Badnell N R 1995 *Phys. Rev. A* **52** 1319
 - [39] Ballance C P and Griffin D C 2006 *J. Phys. B: At. Mol. Opt. Phys.* **39** 3617
 - [40] Clementi E and Roetti C 1974 *At. Data Nucl. Data Tables* **14** 177
 - [41] Hibbert A 1975 *Comput. Phys. Commun.* **9** 141
 - [42] Quigley L and Berrington K A 1996 *J. Phys. B: At. Mol. Phys.* **29** 4529
 - [43] Quigley L, Berrington K A and Pelan J 1998 *Comput. Phys. Commun.* **114** 225
 - [44] Ballance C P, Berrington K A and McLaughlin B M 1999 *Phys. Rev. A* **60** R4217
 - [45] Chen M H *et al* 1997 *At. Data Nucl. Data Tables* **65** 289
 - [46] Ferland G J, Korista K T, Verner D A, Ferguson J W, Kingdon J B and Verner E M 1998 *Pub. Astron. Soc. Pac.(PASP)* **110** 761
 - [47] Ferland G J 2003 *Ann. Rev. of Astron. & Astrophys.* **41** 517
 - [48] Kallman T R and Bautista M A 2001 *Astrophys. J. Suppl. Ser.* **134** 139